

PAPER

A pressure difference sensor inspired by fish canal lateral line

To cite this article: Montassar Aidi Sharif and Xiaobo Tan 2019 *Bioinspir. Biomim.* **14** 055003

View the [article online](#) for updates and enhancements.



IOP | ebooks™

Bringing you innovative digital publishing with leading voices to create your essential collection of books in STEM research.

Start exploring the [collection](#) - download the first chapter of every title for free.

Bioinspiration & Biomimetics



PAPER

A pressure difference sensor inspired by fish canal lateral line

Montassar Aidi Sharif^{1,2} and Xiaobo Tan¹

¹ Department of Electrical and Computer Engineering, Michigan State University, East Lansing, MI 48824, United States of America

² Department of Computer Engineering, Technical College-Kirkuk, Northern Technical University (NTU), Kirkuk, Iraq

E-mail: sharim5@msu.edu (MAS) and xbtan@egr.msu.edu (XT)

Keywords: ionic polymer-metal composite, IPMC sensor, artificial lateral line system, canal neuromast, pressure difference sensor

RECEIVED
8 April 2019

REVISED
24 June 2019

ACCEPTED FOR PUBLICATION
5 July 2019

PUBLISHED
29 July 2019

Abstract

It is of interest to exploit the insight from the lateral line system of fish for flow sensing applications. In this paper, a novel fish canal lateral line-inspired pressure difference sensor is proposed by embedding an ionic polymer-metal composite (IPMC) sensor within a canal filled with viscous fluid. Such a sensor could be used by underwater robots and vehicles for object detection, angle of attack measurement, and source localization. Unlike the biological counterpart that has open ends on the surface of the body, the proposed sensor has two pores covered with a latex membrane, which prevents the canal fluid from mixing with the ambient fluid. The design and fabrication of the sensor are presented, where the sensor is integrated with a fish-like body. The sensor output is experimentally characterized as the fish-like body is rotated with respect to a dipole source, which confirms that the sensor is capable of capturing the pressure difference between the two pores. Finite element modeling and simulation that capture fluid-structure interactions and IPMC physics are conducted to shed light on the sensor behavior. Finally, the utility of the sensor in underwater robotics is illustrated via orienting the fish-like body towards the dipole source using feedback from the proposed sensor.

1. Introduction

The lateral line system is a flow-sensing organ that enables a fish to detect the flow field and pressure gradient around its body [1, 2], and it is essential to a variety of fish behaviors, such as localization of prey/predators [3], schooling [4], rheotaxis, energy-efficient swimming, obstacle avoidance, and station holding [5–7]. The lateral line is comprised of arrays of sensors called neuromasts, each of which consists of a bundle of sensory hair cells encapsulated in a gelatinous cupula [8]. Some of these units, known as superficial neuromasts, extend from the fish skin and are exposed directly to the local flow, while the others, known as canal neuromasts, are recessed below the skin in fluid-filled canals and react to the local pressure gradients [9]. The response of the neuromasts, in the form of action potentials, is transmitted to the central nervous system for information processing [10].

The biological lateral line system (superficial and canal) has inspired a number of efforts to create and implement an engineering equivalent for underwater applications. Artificial lateral line systems could provide a novel sensing modality for navigation and

control of underwater robots and vehicles [11–15], swimming gait pattern recognition [16], object tracking [17], dipole localization [18–20], dipole source characterization [21], vortex sensing [22], and stream flow measurement [23]. Different approaches have been introduced in developing artificial lateral lines [24–26]. For example, hair cell-inspired flow sensors, ranging from millimeter to centimeter scales, have been created using micro-fabrication techniques [27, 28], optical transduction [29], a gel-supported lipid bilayer [30], and novel sensing materials such as ionic polymer-metal composites (IPMCs) [31–35]. While the majority of the aforementioned work emulates the superficial neuromasts, some limited work has addressed canal-type artificial neuromasts [36–38]. The canal-type neuromasts-based sensing applications have also been explored, including, for example, object localization, and hydrodynamic detection [39–41].

In this work, we present a pressure difference sensor inspired by the canal neuromasts of fish. Such a sensor could be used by underwater robots and vehicles for object detection, angle of attack measurement, and source localization. The hair-cell sensor presented

in this work operates by sensing the flow driven by the pressure difference, as exemplified by several other works in literature [36, 39]. Unlike most of the aforementioned artificial lateral line systems on pressure sensing or object localization, where an array of sensors were used, the proposed sensor utilizes one sensing element embedded in a cupula-like structure, which is immersed in a canal (a ‘semicircular’ channel) filled with a viscous fluid. The employed sensing element, which is an IPMC sensor, serves as an artificial hair cell sensor that produces an electrical output in response to the motion of the cupula. As an illustration, the pressure difference sensor is integrated within a fish-like body, and the two ends of the semicircular channel are ‘pores’ like the ears of a fish. Unlike a fish canal that has open ends to the surface of the body, the two pores of the proposed sensor are covered with a thin latex membrane, to prevent the canal fluid from mixing with the ambient fluid.

Figure 1 shows the schematic of the proposed sensor. Experiments are conducted in an AC flow generated by a dipole source, when the fish-like body is placed at different angles with respect to the dipole. The magnitudes of the IPMC short-circuit current output are extracted from the collected data. It is found that the sensor clearly responds to the pressure difference between the pores. To further understand the sensor behavior, time-dependent 3D finite-element simulation is conducted, where both fluid-structure interactions and IPMC physics are accommodated. With experimentally identified model parameters, the proposed model is able to capture the sensor behavior and shed light on pore membrane deflection and cupula displacement under an oscillatory flow. To further demonstrate the use of the proposed sensor in potential robotic applications, feedback control experiments are conducted, to orient the fish-like body towards the dipole source based on the sensor output, starting from an arbitrary initial orientation. In particular, a sliding discrete Fourier transform (SDFT) algorithm [42, 43] is used to efficiently compute the IPMC sensor magnitude for the feedback control.

Some preliminary results of this work were reported in a conference paper [44], where a U-shaped pressure difference sensor prototype was described and experimentally characterized. This paper represents profound and extensive improvement over [44]. First, the design of the sensor is different—the current paper studies a sensor embedded in a fish-like body, and all experimental results are new. Second, the finite modeling and simulation studies in this paper are based on experimentally identified parameters and include IPMC physics, while the simulation in [44] only addressed mechanical deformation of the sensor and there was no experimental validation of the simulation results. Third, the demonstration of the sensor-enabled orientation feedback control, including controller design, SDFT implementation, and experiments, is another significant extension over [44].

The remainder of the paper is organized as follows. In section 2 the development of the system is first described. The results on experimental characterization of the sensor in a dipole flow are presented and discussed in section 3. The finite-element model and simulation are then presented in section 4. The dipole tracking experiment based on sensor feedback is then presented in section 5. Finally, concluding remarks are provided in section 6.

2. System development

The fish-like structure was produced with a multi-material 3D printer (Objet Connex 350, Stratasys) using a hard material (VeroWhite), and it consisted of two parts, as shown in figure 2. The front part had a semicircular canal (inner diameter 3 cm), to house the cupula (see figure 3(b)), and the two pores (diameter 2 cm) at both ends of the canal would be covered by two membranes. The membrane was made of natural latex rubber (thickness 0.01 cm). The cupula structure was 3D-printed with the same multi-material printer (Objet Connex 350, Stratasys), using the soft material. The cupula structure, as shown in figure 3(b), was printed as one piece and comprised of two parts: a cylinder (length 1.5 cm, radius 0.3 cm) is on top of another cylinder (length 0.5 cm, radius 0.13 cm) with a slot (length 1.7 cm, cross-section of 0.02 cm by 0.2 cm) passing through the two cylinders for housing the IPMC sensor. The IPMC fabrication process followed the traditional impregnation-reduction ion-exchange process [45–48]. Following the IPMC fabrication, an additional step of encapsulation was conducted with a parylene coating of 20 μm , followed by a water drive-in process under 70 °C for three days [49]. Finally, the IPMC sensor was inserted into the cupula structure (in particular, the slot) through the slit at the bottom of the smaller cylinder.

Note that an IPMC beam sensor responds to mechanical stimuli in the direction perpendicular to the beam plane, which induce bending. In the proposed sensor design, the IPMC beam (anchored on the bottom) is mounted such that the fluid movement in the canal will impinge on the beam plane to cause bending and vibration. Such mechanical deformation, in turn, will redistribute the mobile ions within the IPMC and produce detectable signals (for example, open-circuit voltage or short-circuit current). In our work, the short-circuit current is measured.

3. Experimental characterizations

3.1. Experimental setup

The rhythmic movement of the body appendages or the fins can be emulated by a vibrating sphere known as a dipole source. A dipole is often used as a stimulus in the study of a lateral line system or its engineering counterpart. In this paper, we have conducted experiments to examine the proposed sensor under an

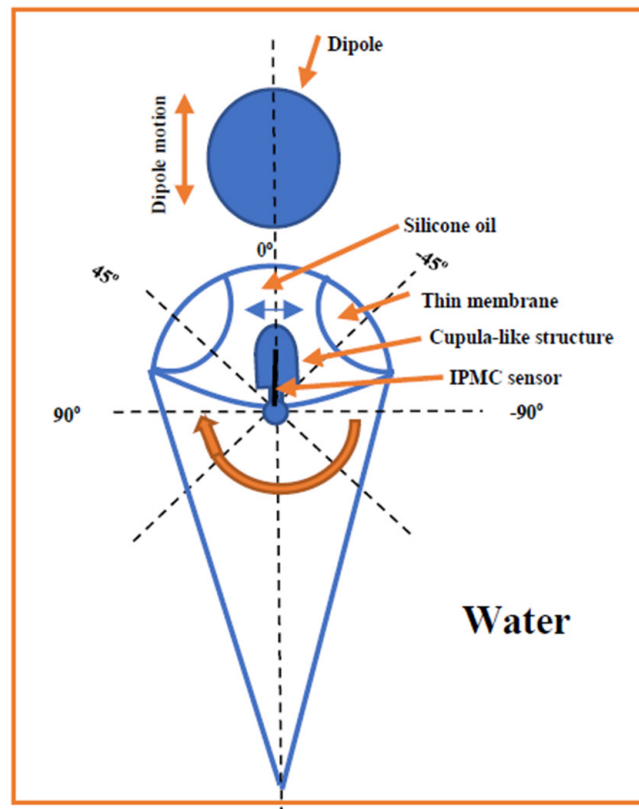


Figure 1. The schematic of the proposed sensor, showing a fish-like structure with two pores on the front and the artificial canal neuromast consisting of an IPMC sensor embedded in a cupula-like structure.

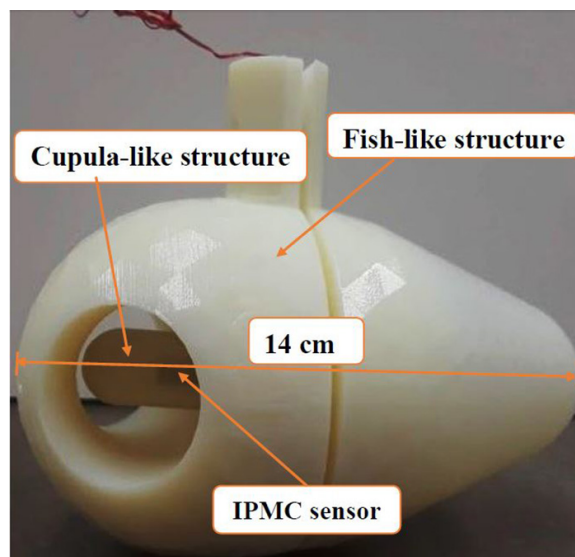


Figure 2. 3D-printed fish-like structure with two pores to be covered with natural latex rubber membranes.

AC flow stimulus generated by a dipole source in a still water tank.

Figure 1 shows a schematic diagram of the proposed sensor and the experimental setup, while figure 4 shows a picture of the major elements that have been used in the experimental setup. Experiments were conducted in a water tank measuring $183 \times 61 \times 61 \text{ cm}^3$. A mini-shaker (Type 4810, Brüel & Kjær) was mounted on an aluminum frame above the tank, generating vibration

(back and forth) on the horizontal plane in a range of 2–30 Hz at a fixed amplitude of electrical input to the mini-shaker. The dipole source used was a metallic sphere with a diameter of 2 cm and it was excited by the mini-shaker. The fish-like structure was fixed to a metal rod via a 3D-printed connector. The top end of the metal rod was fixed on a metal connector, which was rigidly attached to a stepper motor (STM23S-2AE, Applied Motion) used to generate rotation of the

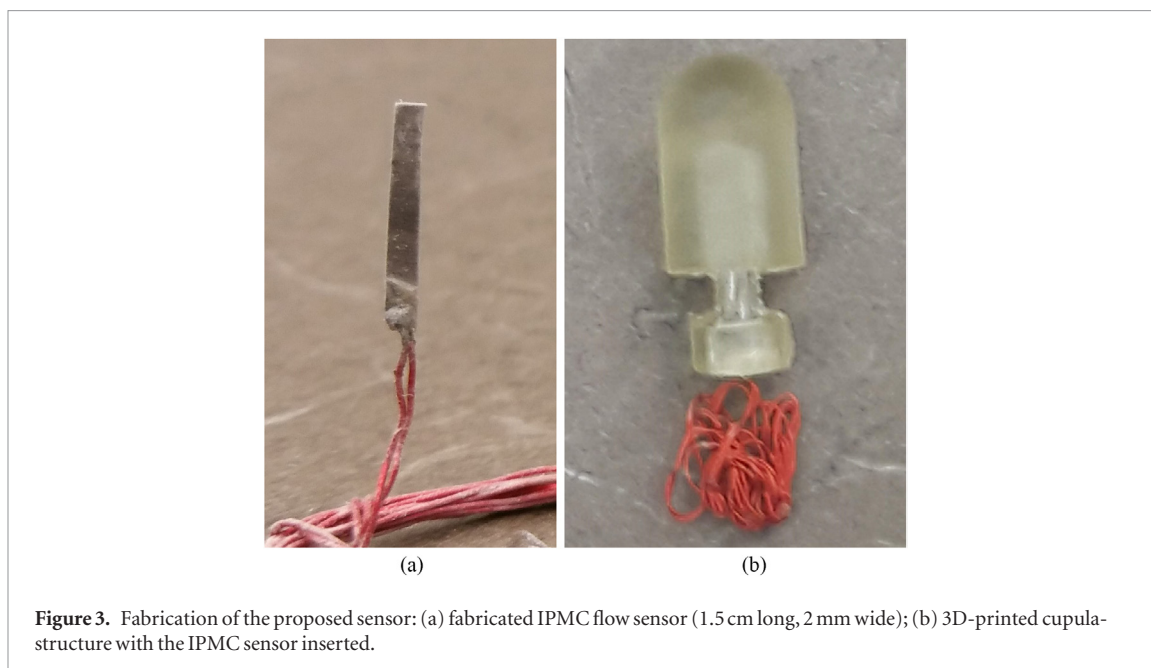


Figure 3. Fabrication of the proposed sensor: (a) fabricated IPMC flow sensor (1.5 cm long, 2 mm wide); (b) 3D-printed cupula-structure with the IPMC sensor inserted.

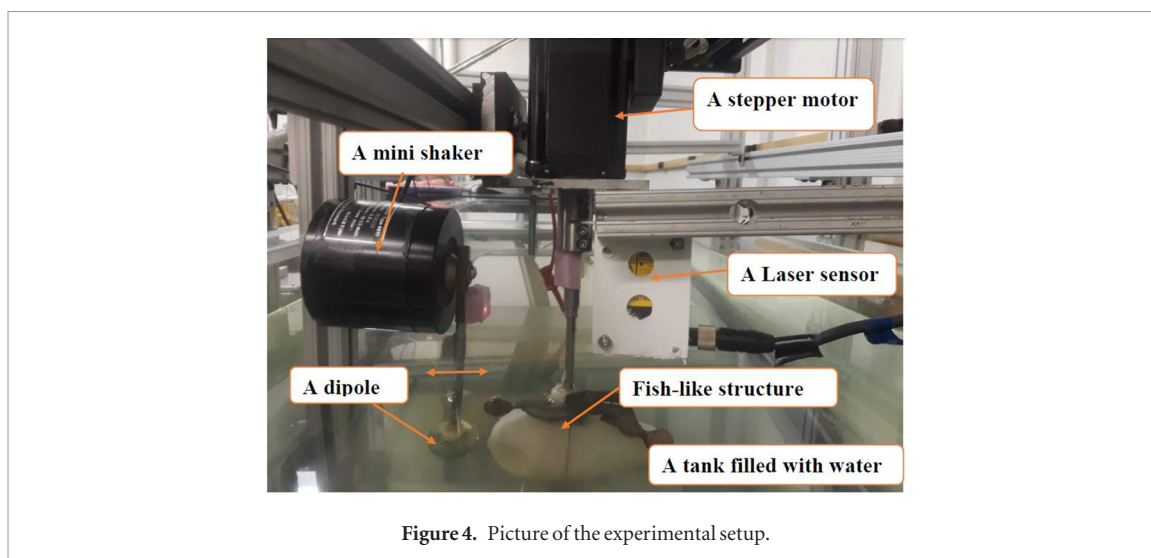


Figure 4. Picture of the experimental setup.

fish-like structure. The stepper motor was controlled via a microcontroller (Arduino-uno). The dipole source and the fish-like structure were completely submerged underwater at a depth of about 20 cm. A laser displacement sensor (OADM 20I6441/S14F, Baumer Electric) was mounted above the water to measure the vibration displacement of the mini-shaker, which was used later in the data processing (see figure 9). The mounting frame for the laser sensor was completely isolated from the frame where the mini-shaker was fixed. The IPMC output was amplified with a two-tier amplification circuit [50] before the acquisition and processing by a lab PC equipped with a dSPACE system (DS 1104, dSPACE).

3.2. Experimental results and discussion

Experiments were first conducted for the case where the dipole source was placed at a fixed point while the fish-like structure was rotated at different angles relative to the dipole source, as illustrated in figure 1.

The sensor was filled with silicone oil, which provides better performance than water as suggested by our earlier work [44]. The frequency of the dipole source was set at 10 Hz. Conceivably, the pressure difference between the two pores would be dependent on the relative dipole location; in particular, the difference is expected to be largest when the dipole is facing one of the membranes and smallest when the dipole is at the midpoint between the pores. Through the pressure difference, the periodic movement of the dipole flow induces the flow movement within the canal and thus the motion of the IPMC-embedded cupula structure, resulting in an IPMC current output at the same frequency as the dipole.

Experiments were first conducted with 2.5 cm separation between the dipole source and the fish-like structure when the two pores are aligned (namely, angle of 0°). We used fast Fourier transform (FFT) to extract the amplitude of the IPMC sensor output corresponding to different angles. Figure 5 shows the

measured IPMC sensor output (short-circuit current) and the spectral content for two cases (0° and 45° relative to dipole). From the figure, it is clear that both signals were oscillatory and nearly periodic. The frequency content in each case was dominated by the dipole frequency (10 Hz) along with minor contribution from the second harmonics. The amplitude of the signal in the 45° case was significantly larger than that in the 0° case. Figure 6 further shows the signal amplitude across the range of angles from -90° to 90° . Experiments were conducted 5 times at each angle, and figure 6 shows both the mean and standard deviation at those angles. One can see that, as either pore approached the dipole source, the sensor output increased. When the dipole was at the midpoint (angle 0°) between the two pores, the IPMC sensor generated the lowest signal, indicating that the pore membranes were vibrating in phase. These results support that the sensor is able to capture the pressure difference between the two pores. The slight asymmetry between the left and right halves of the figure is attributed to the imperfect fabrication of IPMC and the positioning errors for the dipole in the experiments.

Experiments were also conducted with a smaller separation (1 cm) between the dipole and the fish-like structure, and the results (figure 7) show a trend consistent with the case with separation of 1 cm, where the minimum signal amplitude occurring at 0° . The signal amplitude, overall, rises quickly with decreasing dipole-body separation—the maximum amplitude in the case of 1 cm separation is approximately 6 times of that in the case of 2.5 cm. The latter is consistent with the understanding that lateral line sensors work best at close distances.

To further characterize the dynamic behavior of the sensor in detecting the pressure differences, we next conducted experiments where the body was placed at several different angles relative to the dipole source while the dipole vibrated at a range of frequencies. Three angles were chosen to obtain the a frequency response (0° , 30° , and 45°) with a frequency range from 2 to 30 Hz. Each experiment was repeated 5 times to compute the average and the standard deviation.

Figure 8 shows the comparison of the sensitivity of the pressure sensor at different frequencies for the three angles. The sensitivity was obtained by normalizing the magnitude of IPMC sensor output with the magnitude of the dipole velocity, as the latter is directly correlated with the magnitude of the dipole-generated flow field and thus the flow stimulus at the pores. Due to the mini-shaker's own dynamics, the magnitude of displacement of the dipole varies with the frequency given a fixed magnitude for the electrical input to the mini-shaker. In particular, figure 9 shows the measured dipole displacement magnitude at different frequencies, as well as the calculated dipole velocity. The sensitivity of neuromasts is often obtained by normalizing the sensor output with flow velocity or acceleration [51], which is the rationale behind our definition

of the sensitivity in figure 8. From figure 8, it can be seen that the sensitivity of the sensor increases first with the frequency of the dipole until it reaches a maximum at about 12 Hz. The amplitude then drops with the frequency. The peak frequency is likely associated with the resonant frequency of the cupula structure in the fluid. The sensitivity of the sensor in the case of 45° was higher than the case of 30° , which in turn was in general higher than that in the case of 0° . These results further support that this sensor is able to capture the pressure difference at different angular positions.

4. Finite element model and simulation

4.1. Finite element modeling

The response of a canal neuromast, biological or engineered, is due to the cupula deflection in response to a flow field, which is in turn due to a pressure difference between the canal pores. Finite element modeling is essential to the understanding of the sensor behavior and ultimately serving as a tool for design optimization. The modeling of the proposed pressure difference sensor under an oscillatory flow was implemented using COMSOL Multiphysics finite element software packages. The geometry and dimensions of the simulated fish-like structure, the cupula-like structure, and hair cell (IPMC sensor) were exactly the same as to those of the experimental prototype.

The modeling was done in two steps. In the first step a three-dimensional fluid-structure interaction (FSI) module was used to understand the cupula structure and membrane deflection under a dipole stimulus. The second step was to model the IPMC sensor physics and predict its output under bending.

4.1.1. Fluid-structure interaction (FSI)

In the first step of the simulation, FSI physics package was used to model the fluid-structure interaction between the sensor, dipole, and the surrounding water. The canal of the fish-like structure was filled with a fluid, the viscosity of which was five times of that of water and close to that of the biological counterpart. A dipole source was placed outside the canal to create a pressure difference across the pores (see figure 10 for illustration of the simulation setup). Similar to the experimental setting as shown in figure 4, in the simulation setup the fish-like structure could be oriented at different angles relative to the dipole source as seen in figure 11.

The dipole frequency was set to be 10 Hz and the amplitude of the dipole vibration was set to be 0.25 cm. Figure 10 shows a snapshot of the simulated configuration, where the sphere represents the dipole source. The cylinder in the front part of the fish-like structure represents the cupula containing the IPMC sensor. Flexible membranes were attached to the pores. The snapshot in figure 10 shows both the flow field and the displacements of the cupula and membranes while the

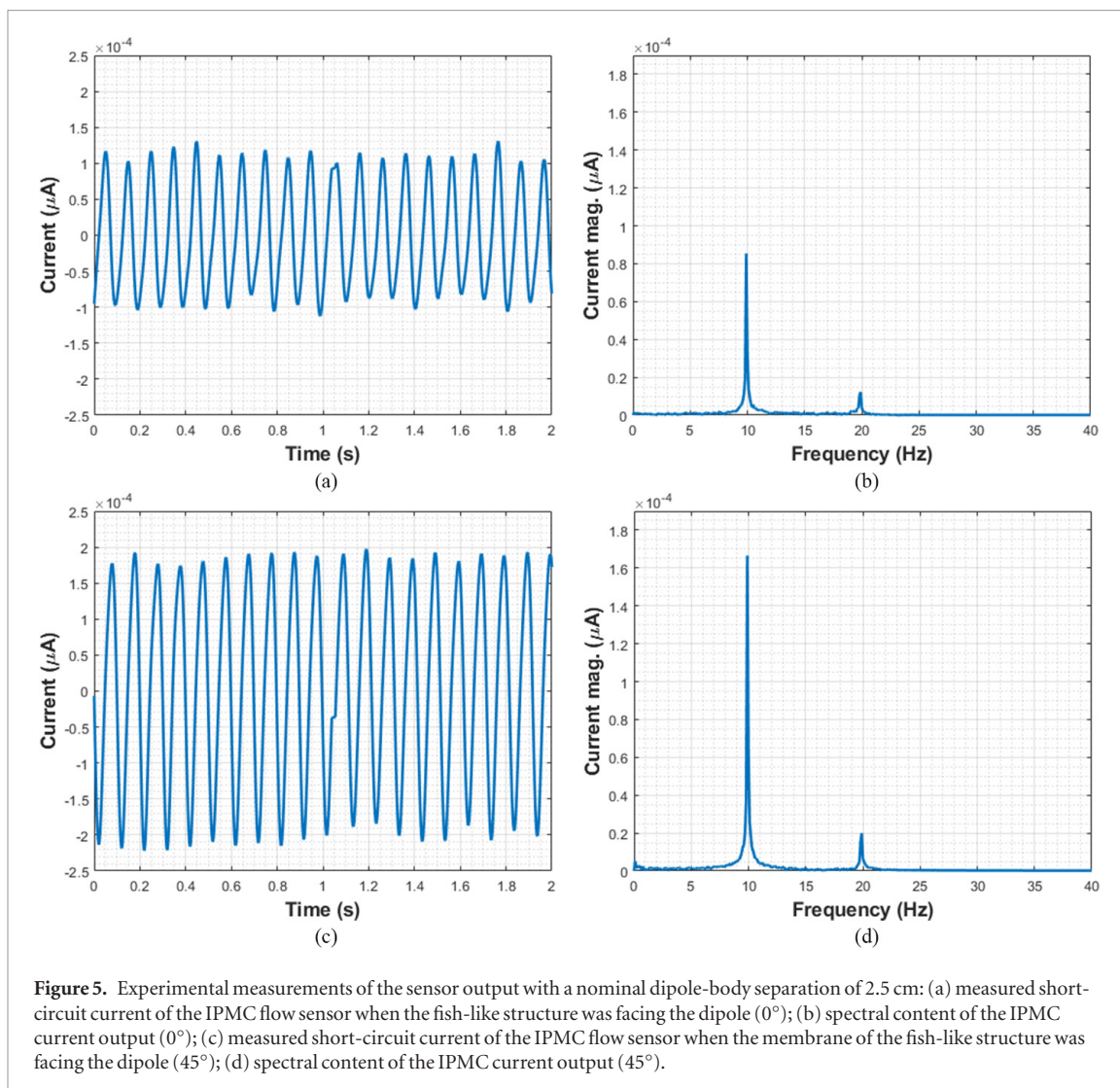


Figure 5. Experimental measurements of the sensor output with a nominal dipole-body separation of 2.5 cm: (a) measured short-circuit current of the IPMC flow sensor when the fish-like structure was facing the dipole (0°); (b) spectral content of the IPMC current output (0°); (c) measured short-circuit current of the IPMC flow sensor when the membrane of the fish-like structure was facing the dipole (45°); (d) spectral content of the IPMC current output (45°).

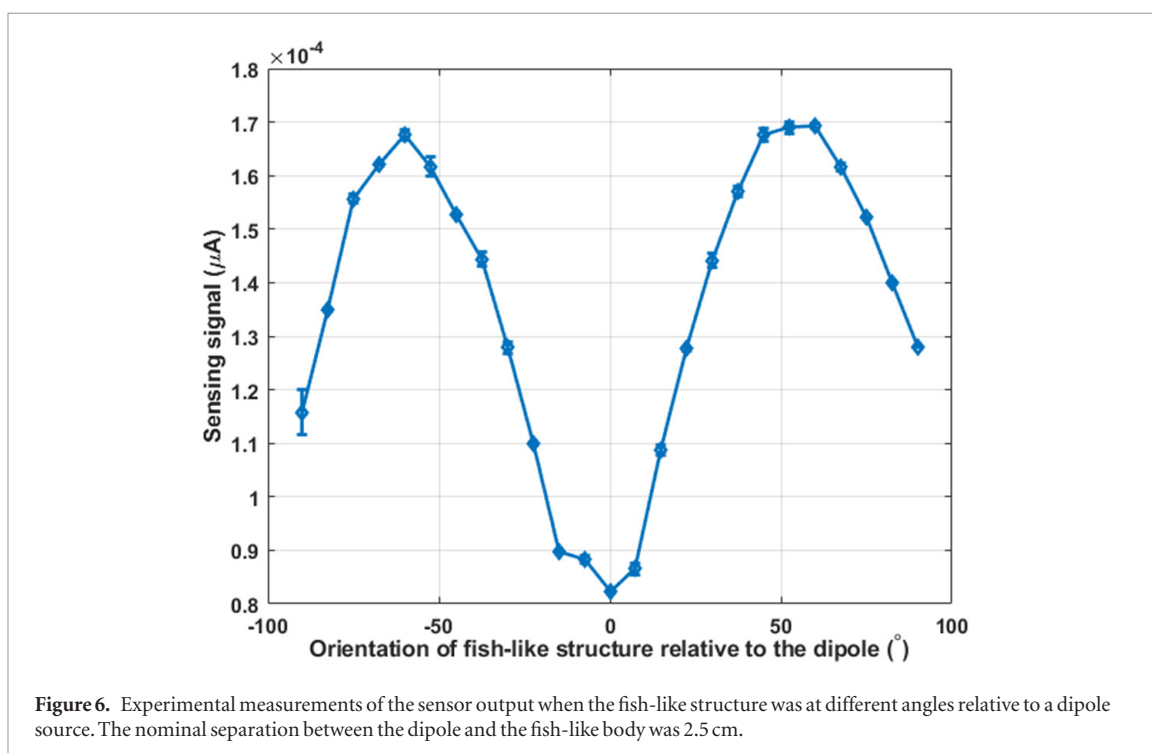


Figure 6. Experimental measurements of the sensor output when the fish-like structure was at different angles relative to a dipole source. The nominal separation between the dipole and the fish-like body was 2.5 cm.

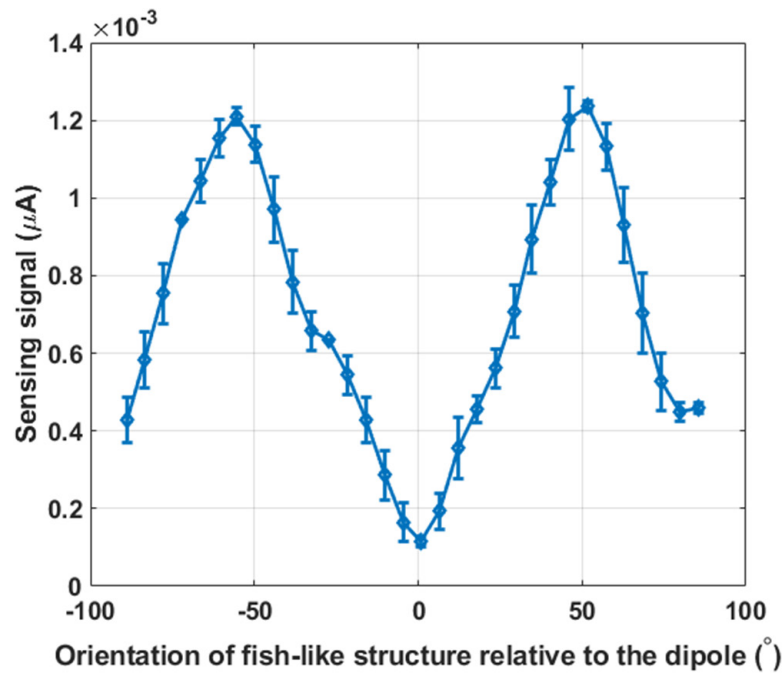


Figure 7. Experimental measurements of the sensor output when the fish-like structure was at different angles relative to the dipole source. The nominal dipole-body separation was 1 cm.

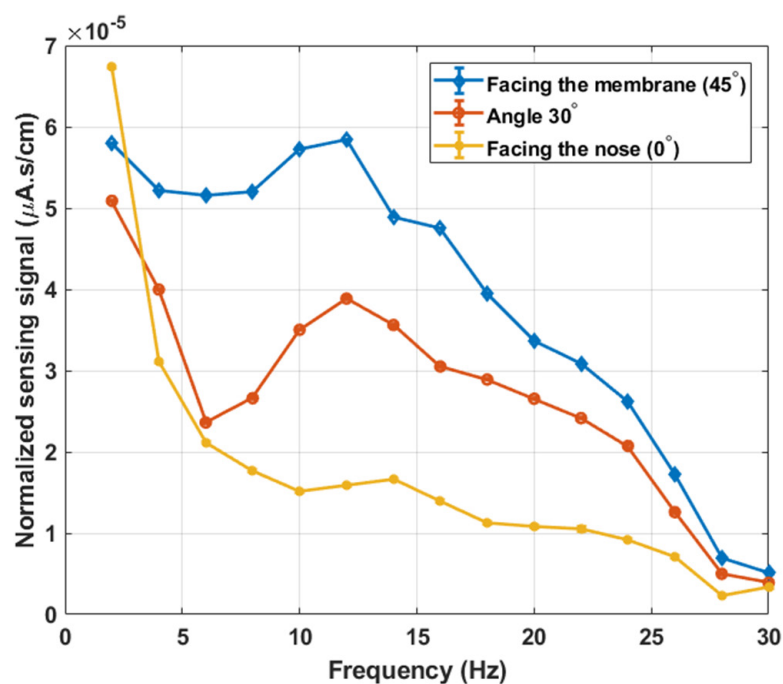


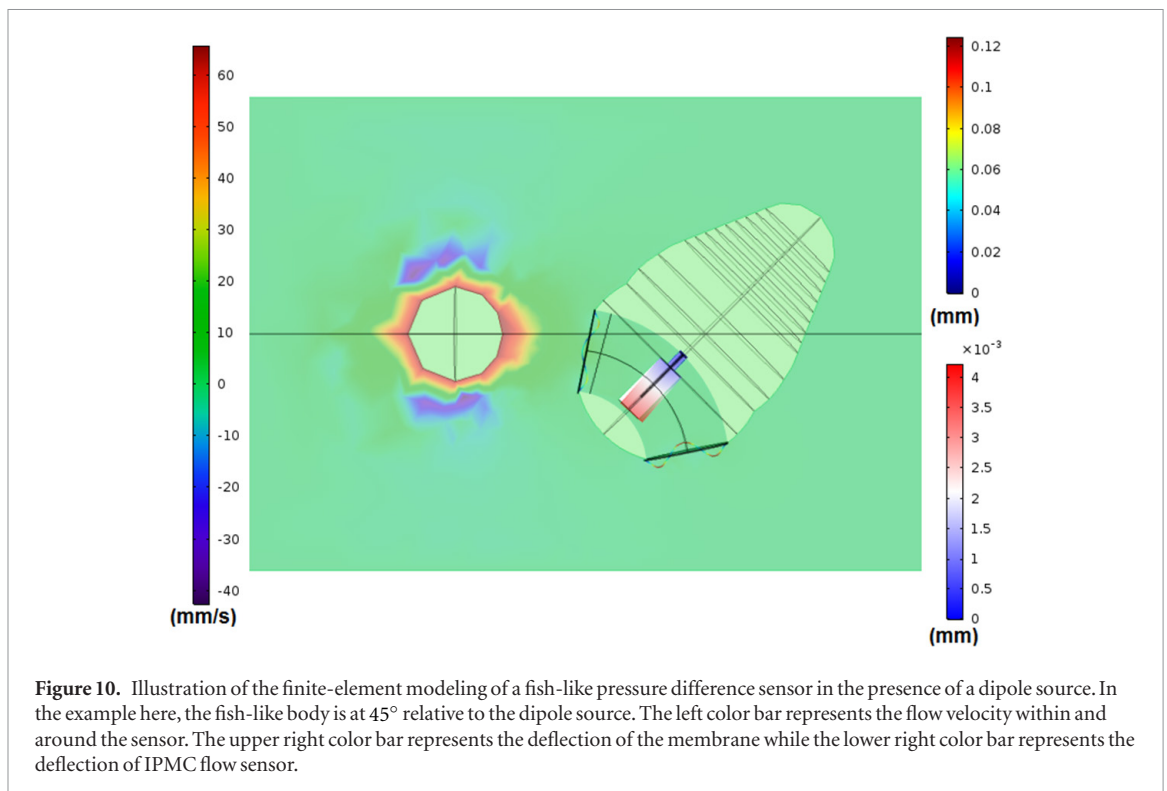
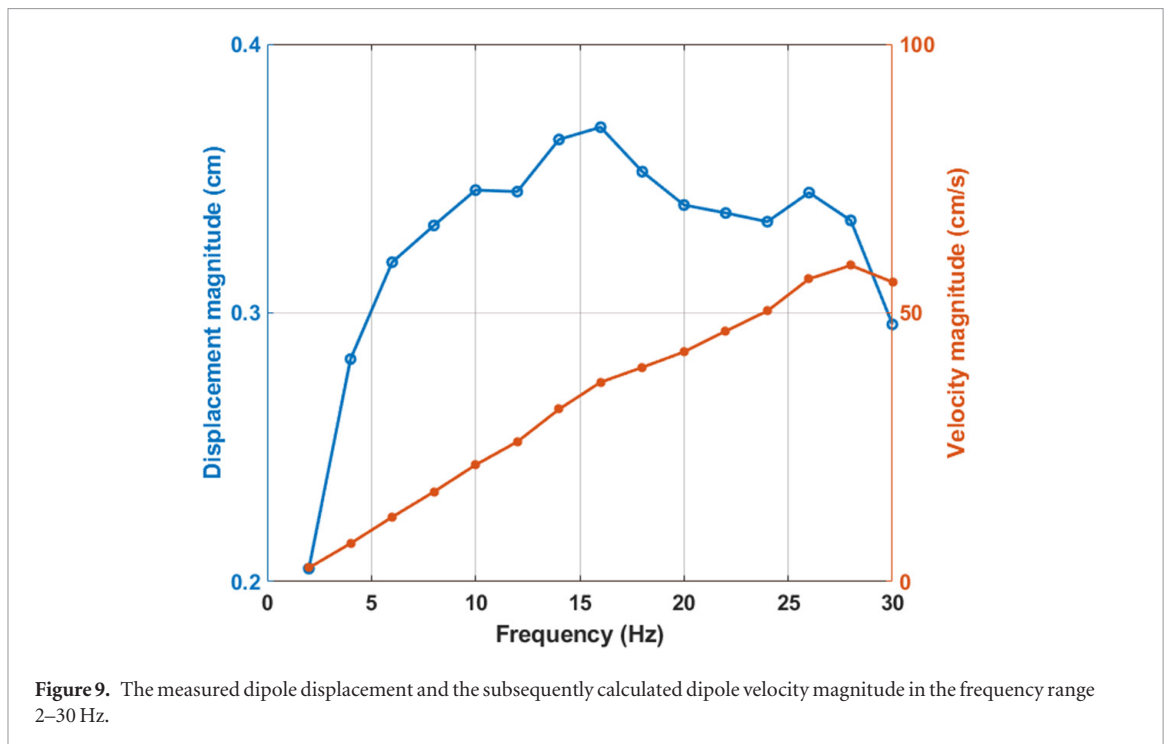
Figure 8. The sensor output is normalized by the dipole velocity at each frequency.

snapshot in figure 12 shows a zoomed-in 3D-deflection of the membranes and the IPMC sensor. Note that the plot was a slice from the three-dimensional model.

4.1.2. IPMC

The modeling of IPMC sensor under oscillatory flow was also conducted using COMSOL Multiphysics finite element software packages. Four physics packages were used to implement the sensor model, which include fluid-structure interaction (FSI),

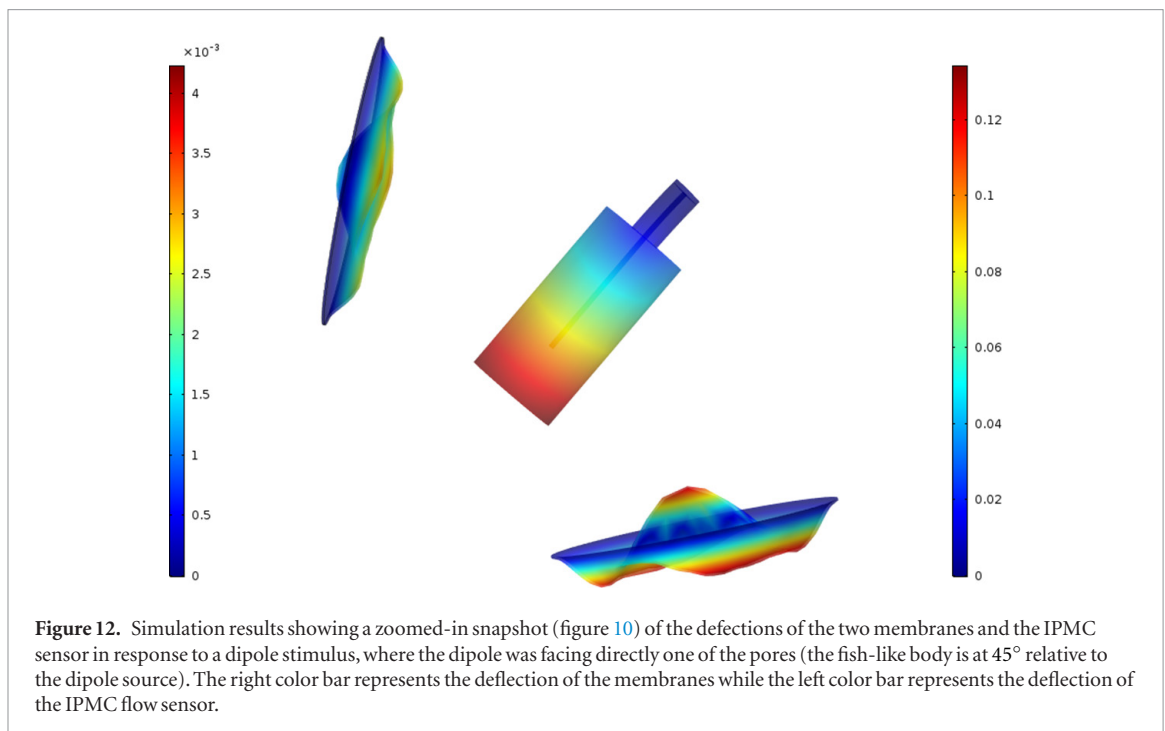
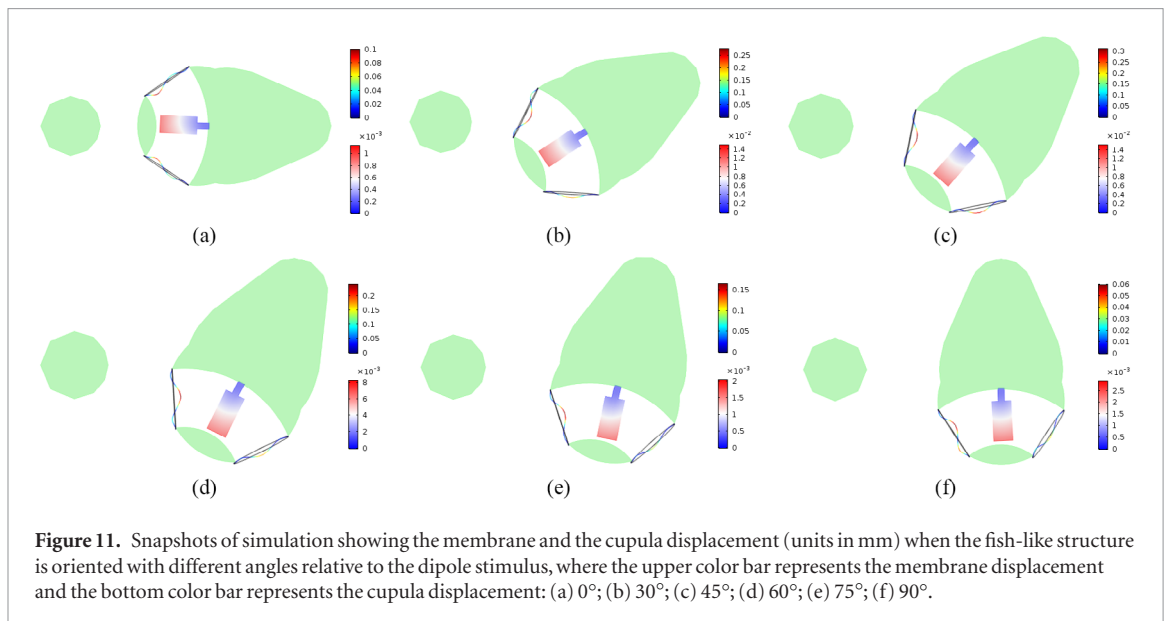
transport of diluted species, general-form PDE to generate the electrical potential within the ion-exchange membrane (Nafion), and electrical current physics. The FSI module was used to describe the flow field and the linear elastic material under bending excitation due to the oscillatory flow inside the canal. The Poisson–Nernst–Planck equation (PNP), which describes the cation concentration and electrical potential dynamics, was realized through the transport of diluted species physics and the general-form PDE



physics modules. The implementation of the IPMC model under bending stimuli was achieved with two separate computations. The deformation of the IPMC sensor due to the dipole flow was calculated first (see section 4.1.1), followed by the execution of the PNP model, which used the deformation data from the first computation as input. A short-circuit current was collected by imposing the electrodes with zero

potential and integrating the collected current density throughout the electrode surface.

The parameters used in simulation were obtained based on the experimental setup. In particular, identification of the IPMC model parameters followed closely the approach described in our prior work [47] the temperature (T), (ρ), the Faraday constant (F), the gas constant (R), the anion concentration C_0 , the Young's



modulus of the IPMC flow sensor (E), and the electrical conductivity of the electrode (σ). The Young's modulus of the cupula-like structure was obtained based on experimental data on the stress/strain relationship collected through a tensile test (see figure 13).

The remaining parameters for the IPMC model, including the diffusion coefficient D and dielectric constant ϵ , were obtained through an artificial neural network-based data fitting process [47], where the data in figure 7 was used. The silicone oil in the canal had a dynamic viscosity of 5.165×10^{-3} Pa s, in comparison to 1.002×10^{-3} Pa s for that of water. Table 1 lists all identified parameters that were used in the simulation.

4.2. Simulation results

Simulation was first conducted for the case where the fish-like structure was oriented at different angles relative to the dipole source with the nominal dipole-body separation of 1 cm, the snapshots of which are shown in figure 11. Each sub-figure in figure 11 also shows the deflections of the pore membranes and the cupula-like structure, where the top color bar represents the membranes deflection (mm) and the lower color bar represents the cupula displacement (mm). In figure 11 we selected six different angles (0°, 30°, 45°, 60°, 75°, 90°) out of 19 different angles (0°–90° with a step of 5°) used in the simulation study. As seen from the figure, when the dipole source

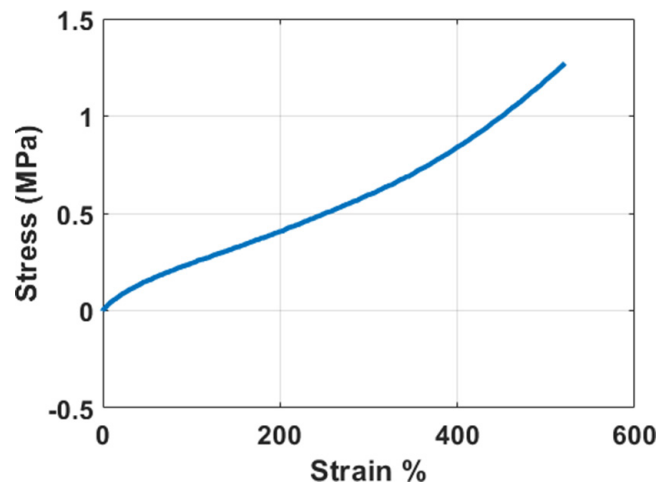


Figure 13. Experimentally obtained stress-strain curve of the cupula structure for estimating Young's modulus.

Table 1. Identified model parameters for the simulation.

F (C mol^{-1})	R ($\text{J mol}^{-1} \text{K}^{-1}$)	T (K)	ν fluid viscosity (Pa s)
96487	8.3143	290	5.165×10^{-3}
D ($\text{m}^2 \text{s}^{-1}$)	C_0 (mol m^{-3})	ϵ (F m^{-1})	σ (S m^{-1})
1×10^{-14}	1050	31×10^{-3}	2200
ρ IPMC (kg m^{-3})	ρ Cupula (kg m^{-3})	E IPMC (Pa)	E Cupula (Pa)
8571.4	1000	5.116×10^8	0.162×10^6

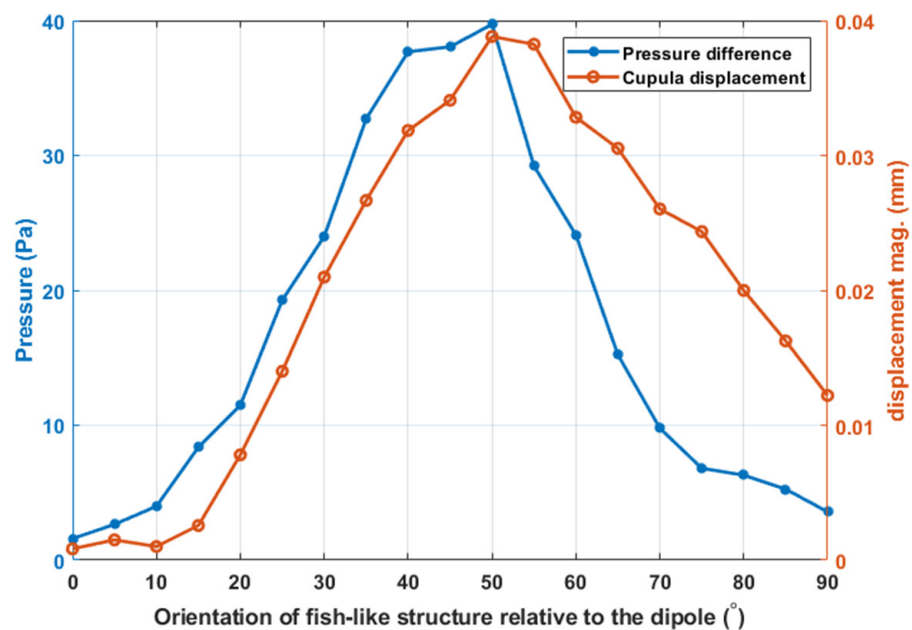


Figure 14. Computed magnitudes for the pressure difference between the two membranes and for the tip displacement of the cupula, respectively.

is located at the midpoint between the two pores (0°), both membranes are fluctuating symmetrically, suggesting minimal pressure difference between the pores and minimal flow of the viscous fluid in the canal, which in turn leads to minimal displacement of the cupula. Figure 14 further shows the tip displacement amplitude of the cupula structure and the magnitude of pressure difference between

the centers of respective pores, as a function of the orientation of the fish-like structure with respect to the dipole source. It can be noted that magnitudes show strong dependency on the orientation of the fish-like body relative to the dipole, with the maximum values occurring around 50° and a trend consistent with the experimentally observed sensor output (shown in figures 6 and 7).

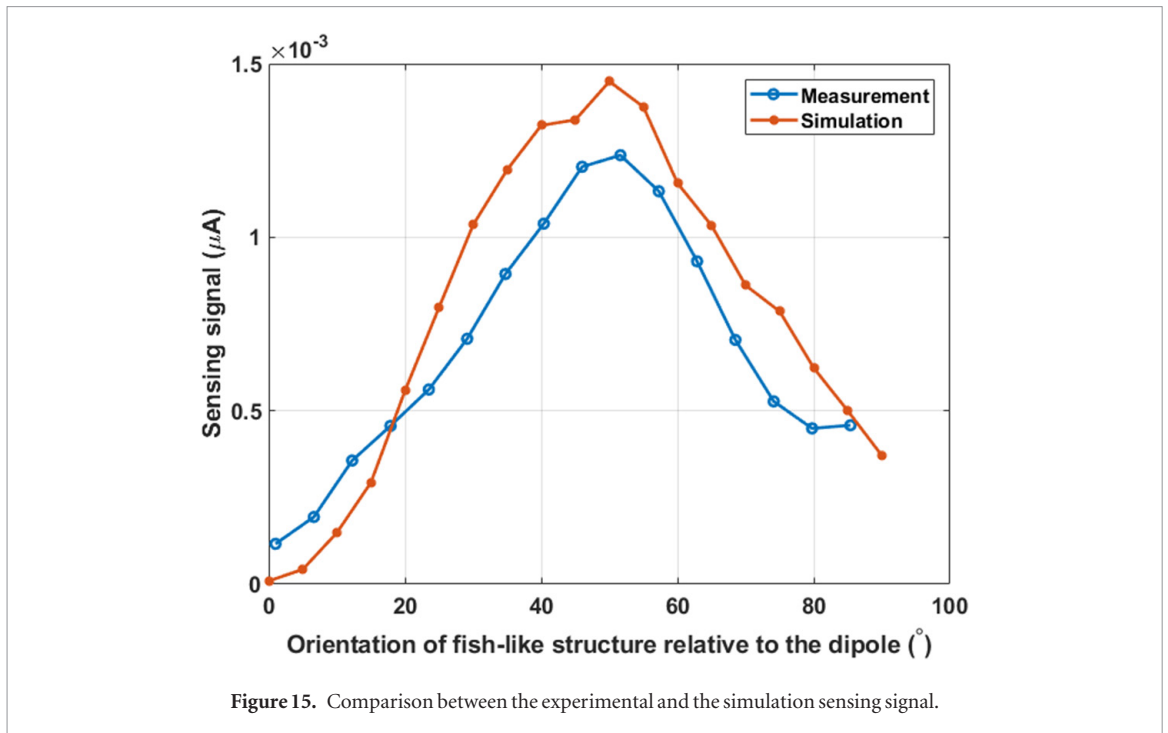


Figure 15. Comparison between the experimental and the simulation sensing signal.

Figure 15 shows the comparison between the measured and simulated sensing signal magnitudes under 10 Hz dipole stimulation. Overall, the figure shows a good agreement between the measurement and simulation. Despite the general good agreement, there are some modest discrepancies between the experimental data and the simulation results, which we attribute mainly to the imperfection in fabrication of the membrane and the IPMC flow sensor, and in the experimental setup.

5. Orientation control of fish-like body with sensor feedback

5.1. Sliding discrete Fourier transform (SDFT) algorithm

In this section the utility of the proposed sensor is illustrated with feedback control of the orientation of the fish-like body using measurement from the pressure difference sensor. Discrete Fourier transform (DFT) can be used to extract the signal magnitudes of the sensor output at different frequencies. However, when the fish-like body rotates, the magnitude of the sensor output evolves with time. The sliding discrete Fourier transform (SDFT) algorithm [42, 43] performs joint time-frequency analysis and is a suitable method for computing a specific spectral bin based on a sliding window of n -time samples.

For a window of N samples, $\{x[n - N - 1], \dots, x[n]\}$, we can evaluate the k th spectral bin using DFT: for $0 \leq k \leq N - 1$

$$X_k[n] = \sum_{m=0}^{N-1} x[n - m + 1 + k] e^{-j2\pi km/N}. \quad (1)$$

Since we are interested in a single frequency f_0 for a dipole stimulus, it suffices to consider a single

frequency bin $k = \lfloor \frac{f_0 N}{F_s} \rfloor$, where $\lfloor \cdot \rfloor$ denotes rounding to the nearest integer and F_s is the sampling frequency used to obtain the sensor signals. The SDFT algorithm can be used to efficiently evaluate X_k recursively as the time index n advances:

$$X_k[n] = e^{-j\omega_0} X_k[n - 1] + x[n] - x[n - N], \quad (2)$$

where $\omega_0 = \frac{2\pi k m}{N}$. The magnitude of $X_k[\cdot]$ represents the signal amplitude at f_0 .

5.2. Feedback controller

The proposed algorithm aims to orient the fish-like structure towards the dipole source (see figure 11(a)), starting from an arbitrary initial orientation. In particular, it uses the magnitude of the IPMC sensing signal to guide the rotation of the fish-like body. In the experiments the fish-like body was initialized at an arbitrary orientation within the range $[-45^\circ, 45^\circ]$, and the goal was to drive it towards 0° , namely, orienting towards the dipole, based on the measurement of the pressure difference sensor. Since the sensor output is a convex function of the orientation angle with the global minimum located at 0° (see figure 7), a greedy search algorithm was adopted. In particular, at each time instant, the stepper motor will move one step (corresponding to 0.9°), but the rotation direction depends on whether the previous action has led to a decrease or increase of the sensor output. Specifically,

$$U_{n+1} = \text{sign}(X_k(n) - X_k(n - 1)) U_n \quad (3)$$

where U_{n+1} is the next control for the stepper motor, while U_n is the current control at time n . $X_k(n)$ is the current magnitude of the IPMC sensing signal, while $X_k(n - 1)$ is the sensing signal magnitude at the previous time step.

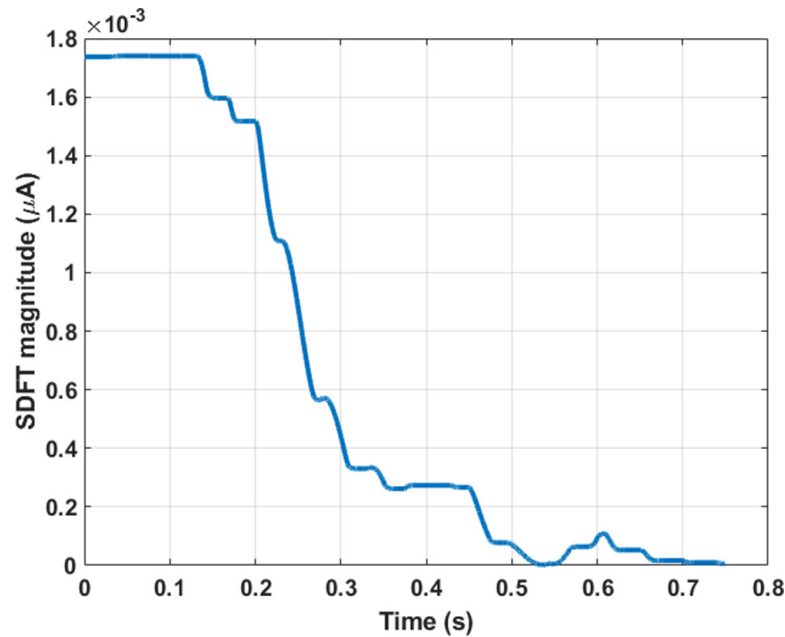


Figure 16. Magnitude trajectory of the IPMC sensor under the feedback control, activated at about $t = 1.3$ s.

Figure 16 shows the evolution of the sensor output magnitude during one experimental run, when the fish-like body started at 45° . It can be seen that, with the feedback from the pressure difference sensor, the body was rotated to 0° in less than 0.5 s, where the sensor output dropped to the level lower than 0.1 nA.

6. Conclusion

In this paper, we presented the fabrication, experimental testing, and simulation of a fish canal lateral line-inspired pressure difference sensor and illustrated its use in underwater applications via a feedback control experiment. The sensor consisted of a 3D-printed rigid semicircular channel and a 3D-printed soft cupula, which housed an IPMC sensor that served as a hair cell. Experimental testing in a dipole flow was conducted to explore performance of the sensor, and the collected data on the IPMC sensor output was analyzed. The experimental results confirmed that the sensor was able to effectively capture the pressure difference between the pores. Finite-element simulation, with parameters identified using experimental data, was conducted to capture the fluid-structure interactions within the proposed sensor. It was found that the simulated displacement of the cupula structure demonstrated similar behavior as observed in the experimental sensor output, when the sensor was oriented at different angles relative to the dipole source. A sliding discrete Fourier transform (SDFT) algorithm was used to effectively compute the IPMC sensor magnitude, which enabled real-time feedback control of the orientation of the fish-like body.

While one could use a pair of commercially available pressure sensors to obtain the pressure difference

measurement, the proposed sensor has several merits. First, if one uses a pair of pressure sensors, good calibration of both sensors is required to just extract the correct polarity of the pressure difference. In contrast, the sensor reported in this paper has a simple operation principle and does not have as stringent requirements on calibration. In addition, the study of such bio-inspired sensors, as a physical model, could help understand the mechanism of biological canal-type lateral line system. In this work we focus on proof of the concept for the sensor, and the relatively large size of the pores is adequate. If one is interested in higher spatial resolution, for example, the pressure differences between different ‘points’ of a structure, down-scaling of the sensor (in particular, the pore size) could be investigated.

For future work, further simulation analysis will be conducted to optimize the geometry and materials of different parts of the sensor. In addition, other applications of the proposed sensor will be explored, including, for example, rheotaxis (alignment with upstream flow), identification of an obstacle in a flow, and localization and tracking of a moving dipole source using potentially two or more pressure difference sensors. These applications will further illustrate the utility of the proposed sensor in underwater navigation and control for robots and vehicles.

Finally, we note that, while the closed pores prevent the canal fluid from mixing with the ambient fluid (water) and escaping, they could impede the canal fluid movement especially under quasi-static pressure differences across the pores. The proposed sensor is thus best for capturing a dynamically changing pressure difference. While in any practical scenarios the pressure difference is likely varying all the time, a sensor with open pores (thus canal filled with ambient

fluid, i.e. water) does have the advantage of producing larger deflection of the cupula under quasi-static pressure differences. Therefore, it is worthwhile to explore the comparison of open-pore and closed-pore designs under those scenarios.

Acknowledgments

This work was supported in part by the Office of Naval Research (N000141210149). The work of Sharif was also supported by the Higher Committee for Education Development in Iraq (HCED).

ORCID iDs

Montassar Aidi Sharif  <https://orcid.org/0000-0002-9879-0631>

Xiaobo Tan  <https://orcid.org/0000-0002-5542-6266>

References

- [1] Coombs S 2002 Imaging of the hydrodynamic environment by the peripheral lateral line system *Bioacoustics* **12** 148–50
- [2] Coombs S 2001 Smart skins: information processing by lateral line flow sensors *Autonomous Robots* **11** 255–61
- [3] Pohlmann K, Atema J and Breithaupt T 2004 The importance of the lateral line in nocturnal predation of piscivorous catfish *J. Exp. Biol.* **207** 2971–8
- [4] Pitcher T J, Partridge B L and Wardle C 1976 A blind fish can school *Science* **194** 963–5
- [5] Von Campenhausen C, Riess I and Weissert R 1981 Detection of stationary objects by the blind cave fish *Anoptichthys jordani* (Characidae) *J. Comparative Physiol.* **143** 369–74
- [6] Bleckmann H 1994 *Reception of Hydrodynamic Stimuli in Aquatic and Semiaquatic Animals* (New York: G. Fischer Verlag)
- [7] Bleckmann H 1986 Role of the lateral line in fish behaviour *The Behaviour of Teleost Fishes* (New York: Springer) pp 177–202
- [8] Coombs S, Janssen J and Webb J C 1988 Diversity of lateral line systems: evolutionary and functional considerations *Sensory Biology of Aquatic Animals* ed J Atema *et al* (New York: Springer) ch 22, pp 553–93
- [9] Kroese A and Schellart N 1992 Velocity- and acceleration-sensitive units in the trunk lateral line of the trout *J. Neurophysiol.* **68** 2212–21
- [10] Bleckmann H 2008 Peripheral and central processing of lateral line information *J. Comparative Physiol. A* **194** 145–58
- [11] Xu Y and Mohseni K 2013 Fish lateral line inspired hydrodynamic feedforward control for autonomous underwater vehicles *IEEE/RSJ Int. Conf. on Intelligent Robots and Systems (IROS)* (IEEE) pp 3565–870
- [12] Yang Y, Nguyen N, Chen N, Lockwood M, Tucker C, Hu H, Bleckmann H, Liu C and Jones D L 2010 Artificial lateral line with biomimetic neuromasts to emulate fish sensing *Bioinspiration Biomimetics* **5** 016001
- [13] Xu Y and Mohseni K 2017 A pressure sensory system inspired by the fish lateral line: hydrodynamic force estimation and wall detection *IEEE J. Ocean. Eng.* **42** 532–43
- [14] De Vries L, Lagor F D, Lei H, Tan X and Paley D A 2015 Distributed flow estimation and closed-loop control of an underwater vehicle with a multi-modal artificial lateral line *Bioinspiration Biomimetics* **10** 025002
- [15] Fan Z, Chen J, Zou J, Bullen D, Liu C and Delcomyn F 2002 Design and fabrication of artificial lateral line flow sensors *J. Micromech. Microeng.* **12** 655
- [16] Liu H, Zhong K, Fu Y, Xie G and Zhu Q 2014 Pattern recognition for robotic fish swimming gaits based on artificial lateral line system and subtractive clustering algorithms *Sensors Transducers* **182** 207
- [17] Ahrari A, Lei H, Sharif M A, Deb K and Tan X 2016 Optimum design of artificial lateral line systems for object tracking under uncertain conditions *GECCO (Companion)* pp 123–4
- [18] Ji M, Zhang Y, Zheng X, Lin X, Liu G and Qiu J 2018 Resolution improvement of dipole source localization for artificial lateral lines based on multiple signal classification *Bioinspiration Biomimetics* **14** 016016
- [19] Abdulsadda A T and Tan X 2013 Nonlinear estimation-based dipole source localization for artificial lateral line systems *Bioinspiration Biomimetics* **8** 026005
- [20] Liu G, Gao S, Sarkodie-Gyan T and Li Z 2018 A novel biomimetic sensor system for vibration source perception of autonomous underwater vehicles based on artificial lateral lines *Meas. Sci. Technol.* **29** 125102
- [21] Ahrari A, Lei H, Sharif M A, Deb K and Tan X 2017 Reliable underwater dipole source characterization in 3D space by an optimally designed artificial lateral line system *Bioinspiration Biomimetics* **12** 036010
- [22] Ren Z and Mohseni K 2012 A model of the lateral line of fish for vortex sensing *Bioinspiration Biomimetics* **7** 036016
- [23] Abels C, Quattieri A, De Vittorio M, Megill W and Rizzi F 2016 A bio-inspired real-time capable artificial lateral line system for freestream flow measurements *Bioinspiration Biomimetics* **11** 035006
- [24] Zheng X, Wang C, Fan R and Xie G 2017 Artificial lateral line based local sensing between two adjacent robotic fish *Bioinspiration Biomimetics* **13** 016002
- [25] Lagor F D, DeVries L D, Waychoff K M and Paley D A 2013 Bio-inspired flow sensing and control: autonomous rheotaxis using distributed pressure measurements *J. Unmanned Syst. Technol.* **1** 78–88
- [26] Nelson K and Mohseni K 2017 Design of a 3D printed, modular lateral line sensory system for hydrodynamic force estimation *Mar. Technol. Soc. J.* **51** 103–15
- [27] Liu C 2007 Micromachined biomimetic artificial haircell sensors *Bioinspiration Biomimetics* **2** S162–9
- [28] Kottapalli A G P, Asadnia M, Miao J and Triantafyllou M 2014 Touch at a distance sensing: lateral-line inspired MEMS flow sensors *Bioinspiration Biomimetics* **9** 046011
- [29] Klein A and Bleckmann H 2011 Determination of object position, vortex shedding frequency and flow velocity using artificial lateral line canals *Beilstein J. Nanotechnol.* **2** 276–83
- [30] Sarles S A and Leo D J 2011 Hair cell sensing with encapsulated interface bilayers *Bioinspiration, Biomimetics, and Bioreplication* vol 7975 (International Society for Optics and Photonics) p 797509
- [31] Abdulsadda A T and Tan X 2013 Underwater tracking of a moving dipole source using an artificial lateral line: algorithm and experimental validation with ionic polymer-metal composite flow sensors *Smart Mater. Struct.* **22** 045010
- [32] Lei H, Li W and Tan X 2012 Microfabrication of IPMC cilia for bio-inspired flow sensing *Electroactive Polymer Actuators and Devices (EAPAD) XIV (Proc. of SPIE vol 8340)* ed Y Bar-Cohen (Bellingham, WA: SPIE) p 83401A
- [33] Lei H and Tan X 2013 Fabrication and characterization of a two-dimensional IPMC sensor *Electroactive Polymer Actuators and Devices (EAPAD) (Proc. of SPIE vol 8687)* ed Y Bar-Cohen (San Diego, CA: SPIE) p 868707
- [34] Lei H, Sharif M A, Paley D A, McHenry M J and Tan X 2016 Performance improvement of IPMC flow sensors with a biologically-inspired cupula structure *Electroactive Polymer Actuators and Devices (EAPAD) vol 9798* (International Society for Optics and Photonics) p 979827
- [35] Abdulsadda A T and Tan X 2012 An artificial lateral line system using IPMC sensor arrays *Int. J. Smart Nano Mater.* **3** 226–42
- [36] Kaldenbach F, Klein A and Bleckmann H 2019 Form-function relationship in artificial lateral lines *Bioinspiration Biomimetics* **14** 026001
- [37] Sharif M A, McHenry M J and Tan X 2017 Modeling of a bio-inspired canal-type lateral line system *ASME 2017 Conf. on Smart Materials, Adaptive Structures and Intelligent Systems* (American Society of Mechanical Engineers) paper SMASIS2017–3756

- [38] Herzog H, Steltenkamp S, Klein A, Tätzner S, Schulze E and Bleckmann H 2015 Micro-machined flow sensors mimicking lateral line canal neuromasts *Micromachines* **6** 1189–212
- [39] Yang Y, Klein A, Bleckmann H and Liu C 2011 Artificial lateral line canal for hydrodynamic detection *Appl. Phys. Lett.* **99** 023701
- [40] van Netten S M 2006 Hydrodynamic detection by cupulae in a lateral line canal: functional relations between physics and physiology *Biol. Cybern.* **94** 67–85
- [41] Chen J, Engel J, Chen N, Pandya S, Coombs S and Liu C 2006 Artificial lateral line and hydrodynamic object tracking *Istanbul. 19th IEEE Int. Conf. on Micro Electro Mechanical Systems (IEEE)* pp 694–7
- [42] Jacobsen E and Lyons R 2003 The sliding DFT *IEEE Signal Process. Mag.* **20** 74–80
- [43] Shatara S and Tan X 2010 An efficient, time-of-flight-based underwater acoustic ranging system for small robotic fish *IEEE J. Ocean. Eng.* **35** 837–46
- [44] Sharif M A and Tan X 2018 A pressure gradient sensor inspired by the canal neuromasts of fish *Electroactive Polymer Actuators and Devices (EAPAD) XX* vol 10594 (International Society for Optics and Photonics) p 105941P
- [45] Lei H, Sharif M A and Tan X 2016 Dynamics of omnidirectional IPMC sensor: experimental characterization and physical modeling *IEEE/ASME Trans. Mechatronics* **21** 601–12
- [46] Kim K J and Shahinpoor M 2003 Ionic polymer-metal composites: II. Manufacturing techniques *Smart Mater. Struct.* **15** 65–79
- [47] Sharif M A, Lei H, Al-Rubaiai M K and Tan X 2018 Ionic polymer-metal composite torsional sensor: physics-based modeling and experimental validation *Smart Materials and Structures* **27** 075039
- [48] Sharif M A and Tan X 2018 IPMC flow sensor exploiting self-generated vortices *Electroactive Polymer Actuators and Devices (EAPAD) XX* vol 10594 (International Society for Optics and Photonics) p 105941B
- [49] Lei H, Li W and Tan X 2014 Encapsulation of ionic polymer-metal composite (IPMC) sensors with thick parylene: fabrication process and characterization results *Sensors Actuators A* **217** 1–12
- [50] Ganley T, Hung D L, Zhu G and Tan X 2011 Modeling and inverse compensation of temperature-dependent ionic polymer-metal composite sensor dynamics *IEEE/ASME Trans. Mechatronics* **16** 80–9
- [51] van Netten S M and McHenry M J 2013 The biophysics of the fish lateral line *The Lateral Line System* (New York: Springer) pp 99–119